Confined magnon dispersion in ferromagnetic and antiferromagnetic thin films in a second quantization approach: The case of Fe and NiO

Julio A. do Nascimento [1,*] Adam Kerrigan,[1,2] S. A. Cavill,[1] Demie Kepaptsoglou [3] Quentin M. Ramasse,[4] Phil J. Hasnip,[1] and Vlado K. Lazarov [1,2,†]

[1] *School of Physics, Engineering and Technology, University of York, York YO10 5DD, United Kingdom*

[2] *York-JEOL Nanocentre, University of York, York YO10 5BR, United Kingdom*

[3] *SuperSTEM, Sci-Tech Daresbury Campus and School of Physics, Engineering and Technology, University of York, York YO10 5DD, United Kingdom*

[4] *SuperSTEM, Sci-Tech Daresbury Campus and School of Physics and Astronomy, University of Leeds, Leeds LS2 9JT, United Kingdom*

(Received 13 December 2023; revised 27 February 2024; accepted 18 June 2024; published 8 July 2024)

We present a methodology based on the calculation of the inelastic scattering from magnons via the spin-scattering function in confined geometries such as thin films using a second quantization formalism, for both ferromagnetic and antiferromagnetic materials. The case studies are chosen with an aim to demonstrate the effects of film thickness and crystal orientation on magnon modes, using bcc Fe(100) and NiO with (100) and (111) crystallographic orientations as prototypical systems. Due to the quantization of the quasimomentum, we observe a granularity in the inelastic spectra in the reciprocal space path reflecting the orientation of the thin film. This approach also allows for the capture of softer modes that appear due to the partial interaction of magnetic moments close to the surface in a thin film geometry, in addition to bulk modes. The softer modes are also affected by crystallographic orientation, as illustrated by the different surface-related peaks of the NiO magnon density of states at approximately ∼65 meV for (100) and ∼42 meV for a (111)-oriented film. Additionally, we explore the role of anisotropy, revealing that anisotropy increases the overall hardness of the magnon modes. The introduction of a surface anisotropy produces a shift of the surface-related magnon DOS peak to higher energies with increased surface anisotropy, and in some cases leads to a surface-confined mode.

DOI: 10.1103/PhysRevB.110.024410

I. INTRODUCTION

The study of the collective dynamics of magnetic systems has attracted a great deal of attention, due to the promise of using spin waves to deliver an energetically efficient way to meet the data processing requirements of modern society. This has led to a body of knowledge in a field generally known as magnonics, which encompasses the production, transmission, storage and processing of information using spin-waves [1,2]. Spin waves are dynamic eigen-excitations of magnetically ordered materials, often described in terms of their quanta, or "magnons," much like photons or phonons are the quanta of light or lattice waves, respectively.

The design and optimization of magnonic devices heavily rely on the careful use of specific geometries, particularly emphasizing lower dimensionality, such as thin films. In this context, it becomes imperative to extend current computational methods, traditionally applied to the study of magnons in bulk materials, to take into account effects arising from confined geometries associated with thin films and heterostructures.

As a result, investigations of magnetism in low dimensions serve a dual purpose. First, it offers valuable insights into how the magnetic properties of a solid evolve when transitioning from a three-dimensional (3D) bulk crystal to two, one, or zero-dimensional structures, which often leads to the emergence of unique phenomena not observed in bulk magnets. Second, from a technological standpoint, the incorporation of magnetic materials into modern technologies necessitates their presence in the form of thin films or wires. In fact, low-dimensional magnetic structures play a pivotal role in the broader field of spintronics [3–7].

Previous computational work on magnons has focused on utilizing atomistic spin dynamics [8], or on solving the linearized equation of motion that derives from the Heisenberg Hamiltonian via a so-called confined ansatz [9,10]. Using the latter approach, a study of magnon confinement effects in low-dimensional magnetic structures was recently reported [11]. Furthermore, in this work, the authors utilized the Holstein-Primakoff transformation [12] and the Bogoliubov transformation [13] to rewrite the spin-scattering function in confined geometries, with calculations performed for a model 1D spin chain.

In the current work, we extend this approach and provide a generalized method for calculating the effect of confinement

*Contact author: julio.nascimento@york.ac.uk
†Contact author: vlado.lazarov@york.ac.uk

in films using the Holstein-Primakoff-transformed Heisenberg Hamiltonian, for systems with known ground states. We note that finding the ground state is a rather challenging task, especially with the introduction of Dzyaloshinskii-Moriya (DM) interaction which is relevant for ultrathin films [14]. We will demonstrate the approach assuming a tensorial exchange formulation and explicitly taking into account anisotropy terms. We note that the dipolar interaction plays an important role in the magnon dispersion for thin films [15,16]. Importantly, the lower symmetry in the dipole-dipole interaction term means that in this case, the Goldstone theorem does not apply, opening the possibility of a nonzero gap in the excitation spectrum [17], that would lead to changes near the Γ point. Here, we are in the short wavelength limit for the magnons, a region dominated by the exchange spin waves [3], hence, the dipolar interaction is omitted in the current work. This approach allows the application of the second quantization to thin films with any spin order, including ferromagnets and antiferromagnets with known ground states. This will open a pathway for calculations that support the broad range of probing methods used to study magnons in technologically relevant thin film systems. We demonstrate this methodology for the prototypical systems of ferromagnetic films of bcc Fe(100) and antiferromagnetic NiO with (100) and (111) crystallographic orientations with varying thicknesses.

II. METHODS

We start by expressing the Heisenberg Hamiltonian with a tensorial exchange parameter $J_{jj'}$ and a magnetocrystalline anisotropy K:

$$H = -\frac{1}{2}\sum_{jj'} \mathbf{S}_j \cdot J_{jj'} \cdot \mathbf{S}_{j'} - K\sum_j (\mathbf{m}\cdot\mathbf{S}_j)^2, \tag{1}$$

where we are modeling an atomistic spin-lattice, usually justified by averaging the fast electron dynamics under an adiabatic approximation [18], assuming that the ground-state is known, with magnetic moments at lattice points labeled by indices j and j' that are represented mathematically by the spin operators, $\mathbf{S}_j$ and $\mathbf{S}_{j'}$. To make explicit the spatial orientation of the spin magnetic moments in the lattice, we will employ the so-called "Kübler's trick" [19–21], whereby we will define the spin operator in the local reference frame ($\bar{\mathbf{S}}_j$), connected to the laboratory reference frame ($\mathbf{S}_j$), by the unitary matrix R_j that defines the spin operators in the local reference frame in which the z direction is parallel to the direction of the expectation value of the local magnetic moment in the ground state, i.e., the quantization axis is defined for each site individually and follows the local classical macrospin orientation, given by

$$\mathcal{R}_j = \begin{pmatrix} \cos\theta_j\cos\phi_j & \cos\theta_j\sin\phi_j & -\sin\theta_j \\ -\sin\phi_j & \cos\phi_j & 0 \\ \sin\theta_j\cos\phi_j & \sin\theta_j\sin\phi_j & \cos\theta_j \end{pmatrix}, \tag{2}$$

such that, $\bar{\mathbf{S}}_j = \mathcal{R}_j \cdot \mathbf{S}_j$, where θ_j and ϕ_j are the polar and azimuthal angles, respectively, of the spin magnetic moments in the laboratory reference frame. Then, the exchange term of the Heisenberg Hamiltonian, the first term in Eq. (1), can be written as

$$\begin{aligned} H_{\text{ex}} &= -\frac{1}{2}\sum_{jj'} \mathbf{S}_j \cdot J_{jj'} \cdot \mathbf{S}_{j'} \\ &= -\frac{1}{2}\sum_{jj'}\sum_{\alpha,\beta,\gamma,\delta} \left(\mathcal{R}_j^{-1}\right)_{\alpha\gamma} \bar{\mathbf{S}}_{j\gamma} (J_{jj'})_{\alpha\beta} \left(\mathcal{R}_{j'}^{-1}\right)_{\beta\delta} \bar{\mathbf{S}}_{j'\delta} \\ &= -\frac{1}{2}\sum_{jj'}\sum_{\alpha,\beta,\gamma,\delta} \bar{\mathbf{S}}_{j\gamma} (\mathcal{R}_j)_{\gamma\alpha} (J_{jj'})_{\alpha\beta} \left(\mathcal{R}_{j'}^{-1}\right)_{\beta\delta} \bar{\mathbf{S}}_{j'\delta} \\ &= -\frac{1}{2}\sum_{jj'} \bar{\mathbf{S}}_j \cdot F_J(j, j') \cdot \bar{\mathbf{S}}_{j'}, \end{aligned} \tag{3}$$

where we have defined

$$F_J(j, j') = \left(\mathcal{R}_j \cdot J_{jj'} \cdot \mathcal{R}_{j'}^{-1}\right) \tag{4}$$

and have used Latin letters to note the lattice sites, and Greek letters for cartesian orientations x, y, and z. Note that this enables us to define a different orientation for each site of a chosen lattice, allowing studies of ferromagnetic and antiferromagnetic materials as well as different spin textures such as spin canting at the surface.

The second component in the Hamiltonian of Eq. (1) characterizes the magnetocrystalline anisotropy, where $\mathbf{m}$ denotes a unit vector specifying the orientation of the magnetocrystalline anisotropy axis. This vector can be expressed in spherical coordinates in the laboratory reference frame as follows:

$$\mathbf{m} = (\sin\eta\cos\delta, \sin\eta\sin\delta, \cos\eta), \tag{5}$$

where η and δ are the polar and the azimuthal angles, respectively.

The use of a tensorial exchange parameter allows the interaction to be modeled in a more general way, where the diagonal terms can be recognized as representing the usual constant exchange interaction, while the off-diagonal terms represent the DM interaction. Therefore, the tensor terms must follow $(J_{jj'})_{\alpha\beta} = -(J_{jj'})_{\beta\alpha}$ for $\alpha \neq \beta$. In other words, the exchange anisotropy manifests itself as an asymmetry in the diagonal terms of the tensorial exchange tensor.

A. Holstein-Primakoff transformation

In the Heisenberg Hamiltonian in Eq. (1), the magnetic moments are modeled by spin operators, $\mathbf{S}_j$ and $\mathbf{S}_{j'}$, which satisfy a $SU(2)$ algebra. A usual step to obtain the magnon dispersion is to rewrite the $SU(2)$ operators as bosonic field operators a_j and $a_j^\dagger$ [20,22,23], which satisfy the following commutation relations:

$$[a_j, a_{j'}^\dagger] = \delta_{jj'}, \tag{6}$$

$$[a_j, a_{j'}] = [a_j^\dagger, a_{j'}^\dagger] = 0. \tag{7}$$

The corresponding Fourier transformed operators a_q and $a_q^\dagger$ correspond to the creation and annihilation of collective oscillations of the magnetic moments, which are interpreted as quasiparticles, the so-called magnons.

The Holstein-Primakoff transformation [12] uses this approach to express the spin operators as

$$\overline{S}_j^x = \frac{\sqrt{2S_j}}{2}(\phi(\hat{n}_j)a_j + a_j^\dagger\phi(\hat{n}_j)), \tag{8}$$

$$\overline{S}_j^y = \frac{\sqrt{2S_j}}{2i}(\phi(\hat{n}_j)a_j - a_j^\dagger\phi(\hat{n}_j)), \tag{9}$$

$$\overline{S}_j^z = S_j - \hat{n}_j, \tag{10}$$

where we set $\hbar = 1$ by convention, S_j is the spin quantum number, and $\hat{n}_j = a_j^\dagger a_j$ is the number operator. Note that we are defining the transformation for the spin operators in the local reference frame. Furthermore, we define $\phi(\hat{n}_j) = \sqrt{1 - \frac{\hat{n}_j}{2S_j}}$ as shorthand notation for convenience.

Considering that the eigenstates of S_j^z are $|S_j, m_{s_j}\rangle$ with eigenvalues $m_{s_j} = S_j, S_j - 1, ..., -S_j$, the number operator $\hat{n}_j$ has eigenstates $|m'_{s_j}\rangle$ where $m'_{s_j} = S_j - m_{s_j}$ with eigenvalues $n_j = 0, 1, 2, ..., 2S_j$. A physical interpretation of this representation is that an increase in the number of magnons signifies a decrease in the z-direction projection of the magnetic moment at a particular site.

The transformation involves the square root of the operators. Formally, this requires an expansion of the form

$$\phi(\hat{n}_j) = 1 - \frac{\hat{n}_j}{4S_j} - \frac{\hat{n}_j^2}{32S_j^2} - \cdots. \tag{11}$$

This leads to a Hamiltonian with an infinite number of terms:

$$H = \sum_{n=0}^{\infty} H_n, \tag{12}$$

where H_n represents a term that involves n operators, e.g., $H_4 \propto a_j^\dagger a_{j'} a_k^\dagger a_l$. In this summation scheme, H_0 represents the ground state, H_1 is zero in systems without DM interaction, and H_2 is the term that carries the spin-wave approximation. Every subsequent term gives rise to multimagnon interactions.

For simplicity, we truncate this series using the linear spin-wave approximation, where only the $n = 2$ term is used, i.e., considering only terms that are quadratic in the operators such that $H_2 \propto a_j^\dagger a_{j'}$. This approximation is justified for temperatures well below the magnetic ordering temperature since it leads to removing interactions between magnons, and in cases where $S \gg 1$, allowing us to neglect higher-order terms in Eq. (11) [23].

B. Fourier transform of bosonic operators

Using the results in the previous subsection we can rewrite the Heisenberg Hamiltonian in the second quantization for an arbitrary magnetic moment orientation. Performing the transformation outlined in Sec. II A, i.e., substituting Eqs. (8)–(10) into Eq. (3), expanding and keeping only terms that involve pairs of creation and annihilation operators, since we are interested in the H_2 term of the Hamiltonian which represents the creation of a single magnon, or a set of noninteracting magnons, we get

$$\begin{aligned} H_2 = -\frac{1}{2}\sum_{jj'}\{&-S_j F_J(j,j')_{zz} a_{j'}^\dagger a_{j'} - S_{j'} F_J(j,j')_{zz} a_j^\dagger a_j \\ &+ \frac{\sqrt{S_j S_{j'}}}{2}[G_1(j,j')a_j^\dagger a_{j'}^\dagger + G_2^*(j,j')a_j^\dagger a_{j'} \\ &+ G_2(j,j')a_j a_{j'}^\dagger + G_1^*(j,j')a_j a_{j'}]\}, \end{aligned} \tag{13}$$

where we have defined the following short-hand notation: $G_1 = F_J(j,j')_{xx} - iF_J(j,j')_{xy} - iF_J(j,j')_{yx} - F_J(j,j')_{yy}$ and $G_2 = F_J(j,j')_{xx} + iF_J(j,j')_{xy} - iF_J(j,j')_{yx} + F_J(j,j')_{yy}$, for the terms of the projection matrix.

Next, we take the Fourier transform of the bosonic operators to exploit the periodicity of the system. In the bulk case, the Fourier transform is applied in all three dimensions of the system. In contrast, in the case of thin films, only two dimensions are Fourier transformed,

$$\begin{aligned} a_{\mathbf{q}_\parallel}^{(r)} &= \frac{1}{\sqrt{N_\parallel}}\sum_j^{(r)} e^{-i\mathbf{q}_\parallel\cdot\mathbf{R}_j} a_j, \\ a_{\mathbf{q}_\parallel}^{(r)\dagger} &= \frac{1}{\sqrt{N_\parallel}}\sum_j^{(r)} e^{i\mathbf{q}_\parallel\cdot\mathbf{R}_j} a_j^\dagger, \\ a_j &= \frac{1}{\sqrt{N_\parallel}}\sum_{q_\parallel} e^{i\mathbf{q}_\parallel\cdot\mathbf{R}_j} a_{q_\parallel}^{(r)}, \\ a_j^\dagger &= \frac{1}{\sqrt{N_\parallel}}\sum_{q_\parallel} e^{-i\mathbf{q}_\parallel\cdot\mathbf{R}_j} a_{q_\parallel}^{(r)\dagger}. \end{aligned} \tag{14}$$

The wave vector $\mathbf{q}_\parallel$ is only defined in directions within the plane of the film, and the normalization constant $N_\parallel$ is the number of magnetic moments in the system, where r labels the sites within the unit cell and $\mathbf{R}_j$ is the position vector of the jth site. Substituting Eq. (14) within Eq. (13) and using the following identity for the Kronecker δ,

$$\sum_j e^{i(\mathbf{q}_\parallel - \mathbf{q}'_\parallel)\cdot\mathbf{R}_j} = N_\parallel \delta_{\mathbf{q}_\parallel \mathbf{q}'_\parallel}, \tag{15}$$

for $\mathbf{q}_\parallel$, $\mathbf{q}'_\parallel$ any two wave vectors, $\mathbf{R}_j$ a position vector for a site j in a system with N sites. The resulting Hamiltonian matrix is given by

$$\begin{aligned} H_2 = \frac{1}{2}\sum_{q_\parallel}\sum_{rs}\sum_u z_u \Bigg\{\Bigg\{ &S_r F_J(r,s)_{zz} a_{q_\parallel}^{(s)\dagger} a_{q_\parallel}^{(s)} + S_s F_J(r,s)_{zz} a_{q_\parallel}^{(r)\dagger} a_{q_\parallel}^{(r)} - \frac{\sqrt{S_r S_s}}{2}\big[G_1(r,s)\Gamma_{rs}^{*(u)}(q_\parallel) a_{q_\parallel}^{(r)\dagger} a_{-q_\parallel}^{(s)\dagger} \\ &+ G_1^*(r,s)\Gamma_{rs}^{(u)}(q_\parallel) a_{-q_\parallel}^{(r)} a_{q_\parallel}^{(s)} + G_2(r,s)\Gamma_{rs}^{(u)}(q_\parallel) a_{q_\parallel}^{(r)\dagger} a_{q_\parallel}^{(s)} + G_2^*(r,s)\Gamma_{rs}^{*(u)}(q_\parallel) a_{q_\parallel}^{(r)\dagger} a_{q_\parallel}^{(s)}\big]\Bigg\}\Bigg\}. \end{aligned} \tag{16}$$

Equation (16) is then symmetrized, so that the terms contribute equally to all four quadrants of the resulting matrix [20]. This is achieved by duplicating every term, taking the Hermitian conjugate of the duplicate terms and dividing the overall result

by two. The fact that the Hamiltonian is Hermitian allows us to take these steps without any change in the result. This is the so-called "spread it around" trick, giving us

$$H_2 = \frac{1}{4}\sum_{q_\parallel}\sum_{rs}\sum_{u} z_u \Bigg\{\Bigg\{ S_r F_J(r,s)_{zz} a^{(s)\dagger}_{q_\parallel} a^{(s)}_{q_\parallel} + S_s F_J(r,s)_{zz} a^{(r)\dagger}_{q_\parallel} a^{(r)}_{q_\parallel} - \frac{\sqrt{S_r S_s}}{2}\big[G_1(r,s)\Gamma^{(u)}_{rs}(q_\parallel) a^{(r)\dagger}_{q_\parallel} a^{(s)\dagger}_{-q_\parallel}$$
$$+ G_1^*(r,s)\Gamma^{*(u)}_{rs}(q_\parallel) a^{(r)}_{-q_\parallel} a^{(s)}_{q_\parallel} + G_2(r,s)\Gamma^{*(u)}_{rs}(q_\parallel) a^{(r)\dagger}_{q_\parallel} a^{(s)}_{q_\parallel} + G_2^*(r,s)\Gamma^{(u)}_{rs}(q_\parallel) a^{(r)\dagger}_{q_\parallel} a^{(s)}_{q_\parallel}\big]\Bigg\}$$
$$+ \Bigg\{ S_r F_J(r,s)_{zz} a^{(s)}_{-q_\parallel} a^{(s)\dagger}_{-q_\parallel} + S_s F_J(r,s)_{zz} a^{(r)}_{-q_\parallel} a^{(r)\dagger}_{-q_\parallel} - \frac{\sqrt{S_r S_s}}{2}\big[G_1^*(r,s)\Gamma^{*(u)}_{rs}(q_\parallel) a^{(r)}_{-q_\parallel} a^{(s)}_{q_\parallel} + G_1(r,s)\Gamma^{(u)}_{rs}(q_\parallel) a^{(r)\dagger}_{q_\parallel} a^{(s)\dagger}_{-q_\parallel}$$
$$+ G_2^*(r,s)\Gamma^{(u)}_{rs}(q_\parallel) a^{(r)}_{-q_\parallel} a^{(s)\dagger}_{-q_\parallel} + G_2(r,s)\Gamma^{*(u)}_{rs}(q_\parallel) a^{(r)}_{-q_\parallel} a^{(s)\dagger}_{-q_\parallel}\big]\Bigg\}\Bigg\}, \tag{17}$$

where $\Gamma^{(u)}_{rs} = (1/z_u)\sum_{\mathbf{d}_u} e^{-i\mathbf{q}_\parallel\cdot\mathbf{d}_u}$ and $\mathbf{d}_u$ represents one of the z_u different distance vectors denoting the uth nearest neighbors, e.g., first, second, etc. The labels r and s are used to distinguish between various magnetic moments within the unit cell. The magnetocrystalline term can also be rewritten using similar steps. Since every term in Eq. (17) has a pair of creation and annihilation operators, we can write it as a multiplication of a matrix with the numerical values of the system-dependent parameters $F_J(r,s)$ and $\Gamma^{(u)}_{rs}(q_\parallel)$, with two vectors composed of the creation and annihilation operators. We can then write Eq. (17) in a compact form as follows:

$$H_2 = \sum_{q_\parallel} v^\dagger_{q_\parallel}\cdot\mathbf{L}(\mathbf{q}_\parallel)\cdot v_{q_\parallel}, \tag{18}$$

where we defined

$$v^\dagger_{q_\parallel} = \big(a^{(1)\dagger}_{q_\parallel}, ..., a^{(M)\dagger}_{q_\parallel} | a^{(1)}_{-q_\parallel}, ..., a^{(M)}_{-q_\parallel}\big), \tag{19}$$

which has the commutation relation

$$\big[v_{q_\parallel}, v^\dagger_{q'_\parallel}\big] = \mathcal{N}\delta_{q_\parallel,q'_\parallel}$$
$$\big[v_{q_\parallel}, v_{q'_\parallel}\big] = \big[v^\dagger_{q_\parallel}, v^\dagger_{q'_\parallel}\big] = 0, \tag{20}$$

where

$$\mathcal{N} = \begin{pmatrix} I & 0 \\ 0 & -I \end{pmatrix}, \tag{21}$$

with I being the identity matrix with rank half the length of $v^\dagger$.

To diagonalize the Hamiltonian we will use the Bogoliubov transformation. Taking into account the commutation relations in Eq. (20), we obtain the equation of motion for v_q,

$$i\frac{dv_{q_\parallel}}{dt} = -[H_2, v_{q_\parallel}] = \mathcal{L}(\mathbf{q}_\parallel)\cdot v_{q_\parallel}, \tag{22}$$

where $\mathcal{L}(q_\parallel) = L(\mathbf{q}_\parallel)\cdot\mathcal{N}$ where we used $\hbar = 1$.

Assuming that the unit cell has M magnetic moments, the matrix $\mathcal{L}(\mathbf{q}_\parallel)$ will be $2M$-dimensional, such that $\varepsilon_n(\mathbf{q}_\parallel) = \omega_n(\mathbf{q}_\parallel)/2 \geqslant 0$ for $n = 1, \cdots, M$ and $\varepsilon_n(\mathbf{q}_\parallel) = -\omega_n(\mathbf{q}_\parallel)/2 \leqslant 0$ for $n = M+1, \cdots, 2M$, with $\hbar = 1$, i.e., the eigenvalues of $\mathcal{L}$ are related to the eigenenergies of the magnon modes that are allowed in the system for each q. There will be M positive and M negative eigenvalues due to particle-hole symmetry.

We diagonalize $L(\mathbf{q}_\parallel)$ with the unitary transformation $L'(\mathbf{q}_\parallel) = UL(\mathbf{q}_\parallel)U^\dagger$, where $U^\dagger$ is a matrix which columns are the eigenvectors of $\mathcal{L}(\mathbf{q}_\parallel)$, this allows us to write

$$H_2 = \sum_{q_\parallel} \vec{v}^\dagger_{q_\parallel} U^\dagger U\mathbf{L}(\mathbf{q}_\parallel)U^\dagger U\vec{v}_{q_\parallel} = \sum_{q_\parallel} w^\dagger_{q_\parallel} L'(\mathbf{q}_\parallel) w_{q_\parallel}, \tag{23}$$

having defined $w^\dagger_{q_\parallel} = \vec{v}^\dagger_{q_\parallel} U^\dagger$ such that

$$w^\dagger_{q_\parallel} = \big(\alpha^{(1)\dagger}_{q_\parallel}, ..., \alpha^{(M)\dagger}_{q_\parallel} | \alpha^{(1)}_{-q_\parallel}, ..., \alpha^{(M)}_{-q_\parallel}\big). \tag{24}$$

Comparing with Eq. (19) we can define

$$\alpha^{(r)\dagger}_{q_\parallel} = \sum_{n=1}^{N}\big(U^\dagger_{r,n} a^{(n)}_{q_\parallel} + U^\dagger_{r,n+N} a^{(n)\dagger}_{-q_\parallel}\big), \tag{25}$$

$$\alpha^{(r)\dagger}_{-q_\parallel} = \sum_{n=1}^{N}\big(U^\dagger_{r+N,n} a^{(n)}_{q_\parallel} + U^\dagger_{r+N,n+N} a^{(n)\dagger}_{-q_\parallel}\big), \tag{26}$$

while in real space we have

$$a_j = \sum_{n=1}^{N}(U^\dagger_{j,n}\alpha_n + U^\dagger_{j,n+N}\alpha^\dagger_n), \tag{27}$$

$$a^\dagger_j = \sum_{n=1}^{N}(U^\dagger_{j+N,n}\alpha_n + U^\dagger_{j+N,n+N}\alpha^\dagger_n). \tag{28}$$

Expanding H_2 in the new diagonal basis with the eigenfrequencies obtained from the diagonalization of $\mathcal{L}(\mathbf{q}_\parallel)$, H_2 can be written as

$$H_2 = \sum_{n=1}^{M}\sum_{q_\parallel}\omega_n(\mathbf{q}_\parallel)\Big[\alpha^{(n)\dagger}_{q_\parallel}\alpha^{(n)}_{q_\parallel} + \frac{1}{2}\Big]. \tag{29}$$

This approach allows the calculation of observables such as the spin-scattering function, magnetization, etc., for both bulk or thin films, by projecting the second quantized spin operators onto the diagonalized basis of the Hamiltonian α_n and $\alpha^\dagger_n$, using Eqs. (27) and (28).

C. Spin-scattering function

The spin-scattering function is a proxy for neutron-scattering measurements also sometimes called the dynamic

structure factor. It is given by the space and time Fourier transform of the time-dependent spin-spin correlation function:

$$\mathcal{S}_{\alpha\beta}(\mathbf{q},\omega)=\frac{1}{2\pi N}\sum_{j,j'}\int dt e^{-i\omega t}e^{-i\mathbf{q}\cdot(\mathbf{r}_j-\mathbf{r}_{j'})}\left\langle s_j^{\alpha}(0)s_{j'}^{\beta}(t)\right\rangle_T. \tag{30}$$

Here we are noting N as the total number of spins in the lattice. Once more, we employ Latin letters to designate lattice sites, while Greek letters are utilized for denoting Cartesian directions. This way the spin operator s_j^{α} represents the α component of a spin located at position $\mathbf{r}_j$. The $\langle\cdot\rangle_T$ denotes the quantum and thermal average at temperature T.

In this section, the spin-scattering function is connected to the eigenvalues and eigenvectors of $\mathcal{L}$, which give us the frequencies and their spectral weights for the magnons in the system, respectively.

The spin operators in real space can be expressed as

$$s_j^{\alpha}(t)=\sqrt{\frac{S_j}{2}}\{V_{j\alpha}^{-}a_j(t)+V_{j\alpha}^{+}a_j^{\dagger}(t)\}, \tag{31}$$

noting that $a_j(t)=e^{-i\omega_n t}a_j$, with

$$V_{j\alpha}^{\pm}=(\mathcal{R}_j)_{x\alpha}\pm i(\mathcal{R}_j)_{y\alpha}. \tag{32}$$

By substituting Eqs. (31), (27), and (28) in the scattering function Eq. (30), noting that $\langle\alpha_n^{\dagger}\alpha_{n'}^{\dagger}\rangle_T=\langle\alpha_n\alpha_{n'}\rangle_T=0$ and $\langle\alpha_n^{\dagger}\alpha_{n'}\rangle_T=n_B(\omega_n)\delta_{nn'}$, where n_B is the Bose-Einstein distribution, we perform the Fourier transform on the scattering function and focus on the positive energies of the spectrum, to obtain

$$\mathcal{S}_{\alpha\beta}(\mathbf{q},\omega)=\frac{1}{2M}\sum_{n=1}^{M}\sum_{r,s}\frac{\sqrt{S_rS_s}}{2}e^{-iq_{\perp}\cdot(\mathbf{r}_r-\mathbf{r}_s)}\times\left(W_r^{(n)}\right)_{\alpha}\left(W_s^{(n)}\right)_{\beta}[1+n_B]\delta(\omega-\omega_n), \tag{33}$$

where we have defined $q_{\perp}$, as the component of the wave vector in the confinement direction, and defined the shorthand notation:

$$\left(W_r^{(n)}\right)_{\alpha}=(V_{r,\alpha}^{-}U_{r,n}^{\dagger}+V_{r,\alpha}^{+}U_{r+N,n}^{\dagger}), \tag{34}$$

$$\left(W_s^{(n)}\right)_{\beta}=(V_{s,\beta}^{-}U_{s,n+N}^{\dagger}+V_{s,\beta}^{+}U_{s+N,n+N}^{\dagger}). \tag{35}$$

To account for finite instrument $\delta(\omega-\omega_n)$ is replaced by a Gaussian broadening given by

$$\delta(\omega-\omega_n)\to\frac{1}{\sqrt{2\pi\,\Delta^2}}e^{-\frac{(\omega-\omega_n)^2}{2\Delta^2}}. \tag{36}$$

It is important to emphasize that with this method we can evaluate thin films and heterostructures, and also use the parameters such as J_{ij} and anisotropies K for each different layer and between different layers, as required by the physics of the system.

For colinear spins, the calculation of $S_{\alpha\beta}$, where α and β are the Cartesian directions x, y, and z, aligned with the z axis, for cubic unit cells, we have $S_{xx}(q,\omega)=S_{yy}(q,\omega)\neq 0$, while $S_{\alpha\beta}(q,\omega)=S_{zz}(q,\omega)=0$ for $\alpha\neq\beta$.

The spin-scattering function gives a relative measurement of the amount the magnetic moment changes in a particular direction, i.e., if all magnetic moments in the system are pointing in the z direction and start to precess, then only the magnetic moment projections in the x and y directions change, under the spin-wave approximation, which leads to a nonzero value for the $S_{xx}(q,\omega)$ and $S_{yy}(q,\omega)$ and zero value for $S_{zz}(q,\omega)$, assuming the spin-wave approximation.

D. Magnon density of states

To compute the magnon density of states (DOS), a methodology akin to that utilized in the derivation linking the velocity correlation function to the vibrational density of states for phonons [24,25] is used. Analogously, this approach is extended to the spin-spin correlation function. Employing the Holstein-Primakoff transformation, and the change of basis given in Eqs. (31), (27), and (28) in the time-dependent form $\alpha_n(t)=\alpha_n e^{-i\omega_n t}$. where ω_n are the eigenfrequencies of the magnons in the system, the density of states is given by

$$\rho(\omega)\propto\sum_{n=1}^{M}\sum_{q}\sum_{r,s}e^{-i\mathbf{q}_{\perp}\cdot(\mathbf{r}_r-\mathbf{r}_s)}\left(W_r^{(n)}\right)_{\alpha}\left(W_s^{(n)}\right)_{\alpha}\delta(\omega-\omega_n(q)), \tag{37}$$

where Einstein's summation convention is used for the Cartesian orientations labeled by α, and the constants in front were omitted. This approach ensures uniformity in the density of states (DOS), irrespective of the number of magnetic moments within the unit cell representing the system. Each magnetic moment in the unit cell contributes to a distinct mode in the magnon dispersion, with no guarantee of degeneracy. By deriving the DOS through the spin-spin correlation function, distinct weights are assigned to each mode, with a preference for those associated with the primitive cell. This weighting scheme ensures a consistent solution, rendering the final DOS independent of the chosen unit cell for calculation purposes.

III. RESULTS

In this section, examples are provided to show the physics that is captured by the method outlined above. We calculate three different cases of thin films, ferromagnetic bcc Fe (100), antiferromagnetic NiO(100) and NiO(111). We will evaluate numerically the spin-scattering function using Eq. (33), and the magnon DOS by calculating the contribution to the spin-scattering function of all modes on a grid in reciprocal space.

A. bcc Fe(100)

We start with the prototype ferromagnetic material bcc Fe, a well-known and broadly studied system [8,18,26,27].

The calculations performed in this section have used the J_{ij} parameters proposed in Ref. [18], where 25 nearest neighbors are taken into account, for the value of S we used the magnetic moment taken as $2.26\,\mu_B$ [28] which is then divided by the Landè g-factor for a pure spin system.

Figure 1 shows S_{xx} where we used a temperature of 2K, for films of bcc Fe (001) of varying thickness. The sample is assumed to be infinite in the (x,y) plane, and confined to a limited number of monolayers in the z direction, as indicated. As bcc Fe is a cubic system, S_{xx} is the same as S_{yy}. The spin-scattering functions are evaluated for thin films with sizes ranging from 10 to 50 monolayers (ML). In addition, we show

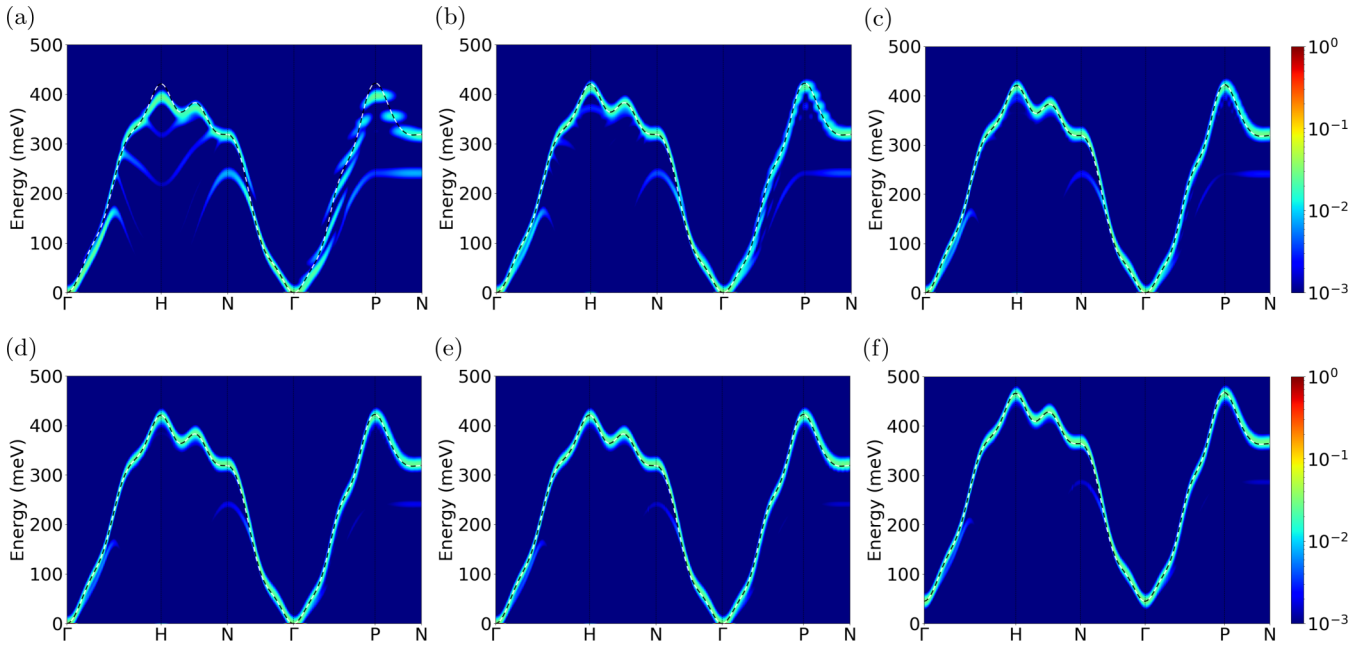

FIG. 1. Spin-scattering function of bcc Fe thin films with (a) 10, (b) 20, (c) 30, (d) 40, and (e) 50 monolayers. (f) 50 monolayers with an added 20 meV of anisotropy in the crystallographic direction of confinement (100), with 25 nearest neighbors and a temperature of 2K was used for all calculations. For comparison, the bulk dispersion is shown as a black/white line. A broadening of $\Delta = 6.5$ meV was used.

the bulk magnon dispersion, calculated using our formulation but for an infinite model in 3D, as a dashed black/white line. The effect of confinement is clearly observed by the emergence of granularity in the spin-scattering function plot, arising from quasimomentum quantization for $q_{\parallel}$ resulting from the finite nature of this direction, as shown along the path traversing the finite z direction ($\Gamma - P - N$). We observe that, since the trajectory deviates from the $q_{\parallel}$ direction, which is the direction of confinement in our thin film geometry, the quantization does not yield symmetrical shapes for the granular features. Instead, they exhibit distinct shapes attributable to the trajectories in reciprocal space that are nonparallel to the finite direction. As we increase the number of monolayers, these granular features become increasingly densely packed, ultimately converging towards a continuous line in the limit of a bulk solid. The thin film calculations therefore tend towards the bulk when the system size increases, as expected in the limit of a large number of layers. We note that the calculated bulk spin-scattering function using our approach agrees well with previous calculations of the magnon dispersion and accompanying experiments for bulk bcc Fe [8,18]. In particular, our results appear to capture the onset of the Kohn anomalies in the path between Γ-H and between H-N, albeit less prominently than in references [8,18], which can be explained due to the fact that we have employed parameters representing next nearest neighbours up to a distance of five times the lattice constant a, whereas prior research had considered parameters extending up to $7a$ as discussed in Refs. [8,18].

The treatment of the Heisenberg Hamiltonian as presented in the methods section above captures the fact that the top and bottom layers (i.e., the surfaces) have fewer neighbors than bulklike layers, resulting in a reduction of interactions, which leads to the appearance of softer modes that are less intense and decrease in intensity as the system increases in size; see Fig. 1. Furthermore, in Fig. 1(f) we show that the addition of $K = 20$ meV of magnetocrystalline anisotropy in the (001) direction parallel to the magnetic moments in the 50 monolayers case, results in a rigid shift in energy for all the modes to higher energies.

The existence of the additional softer surface-related modes can be clearly seen in the magnon DOS calculated using Eq. (37), as shown in Fig. 2, for a thin film of 10 monolayers. This manifests itself by the appearance of a peak around 180 meV, which is not present in the bulk DOS, highlighted by the blue arrow in Fig. 2.

The confined peak in the DOS is dependent on the surface properties. This is illustrated in Fig. 3, where on the top and bottom surfaces of the 10 monolayer Fe film an artificial

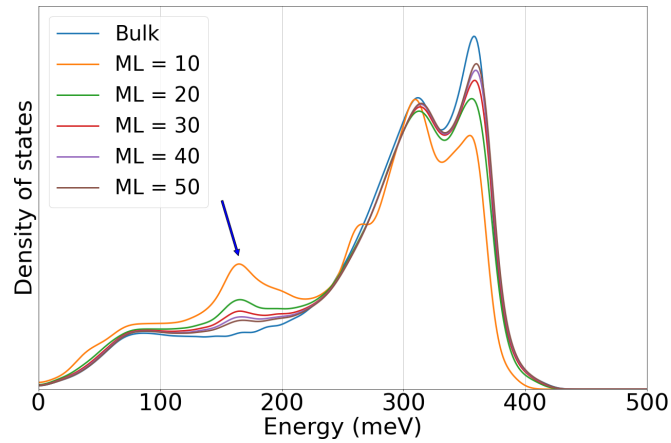

FIG. 2. Density of states of Fe bcc comparing Bulk with varying sizes of thin films with 25 nearest neighbors. A broadening of $\Delta = 6.5$ meV was used.

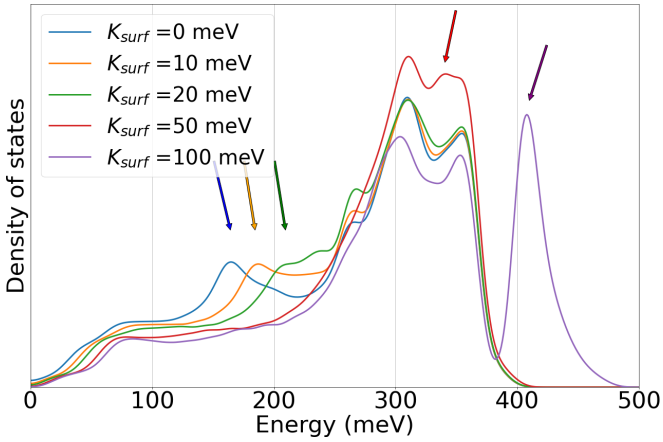

FIG. 3. Density of states of bcc Fe thin film with size 10 monolayers, for varying intensities of K_{surf} with 25 nearest neighbors. A broadening of $\Delta = 6.5$ meV, was used.

surface-only anisotropy (K_{surf}) is added. As K_{surf} increases, the confined DOS peak shifts to higher energies, and eventually becomes localized at energies above the bulk dispersion.

B. NiO(100) and NiO(111)

Next, we consider NiO to demonstrate the applicability of our method to antiferromagnetic thin films. The flexible ability to set the magnetic moments' modulus and directions inside the unit cell allows for the study of both colinear and noncolinear systems, as well as at the interfaces between them.

Exchange parameters from inelastic neutron-scattering experiments suggest that the first-neighbor $J_{1,p} = 1.39$ meV and $J_{1,ap} = 1.35$ meV, where $J_{1,p}$ is the interaction between parallel first neighbors and $J_{1,ap}$ is the interaction between antiparallel first neighbors [29,30]. Similarly, the second-neighbor antiferromagnetic exchange interaction was determined to be $J_2 = -19.01$ meV. The small difference between $J_{1,p}$ and $J_{1,ap}$ was attributed to lattice distortion, as previously pointed out in Refs. [29,30]. The magnetic moment of Ni used in the calculations is $1.4\,\mu_B$ [31].

Figure 4 shows the spin-scattering function for NiO(100) with 5, 10, 15, 20, and 30 monolayers, alongside the bulk NiO case, again represented by the black/white line.

As expected, and similar to bbc Fe, we confirm the tendency to match the bulk case in our calculations as the number of monolayers is increased. A softer energy mode related to the reduced interaction of the magnetic moments at the surfaces also appears for the thin film cases.

In Fig. 4(f) we show that adding $K = 5$ meV of magnetocrystalline anisotropy in the direction of the magnetic moments in the 20 monolayers case results in a shift in energy for all the modes to higher energies. In contrast to the bcc Fe case, this change is not rigid: the lower energies of the modes are affected more than the higher ones.

As with Fe, the magnon DOS of NiO(100) was calculated and is shown in Fig. 5. The calculation confirms the appearance of the confined modes and their relation to the bulk case. The general tendency is of a pronounced confinement-related peak that continuously decreases in intensity with the increase in the number of layers and eventually merges with the bulklike peaks. We note that in the presented range of DOS calculations, only in ultra-thin films, below 10 ML, are the confined modes comparable to or larger than their bulklike counterparts.

The effect of crystallographic direction on confinement is illustrated by a set of complementary calculations carried out

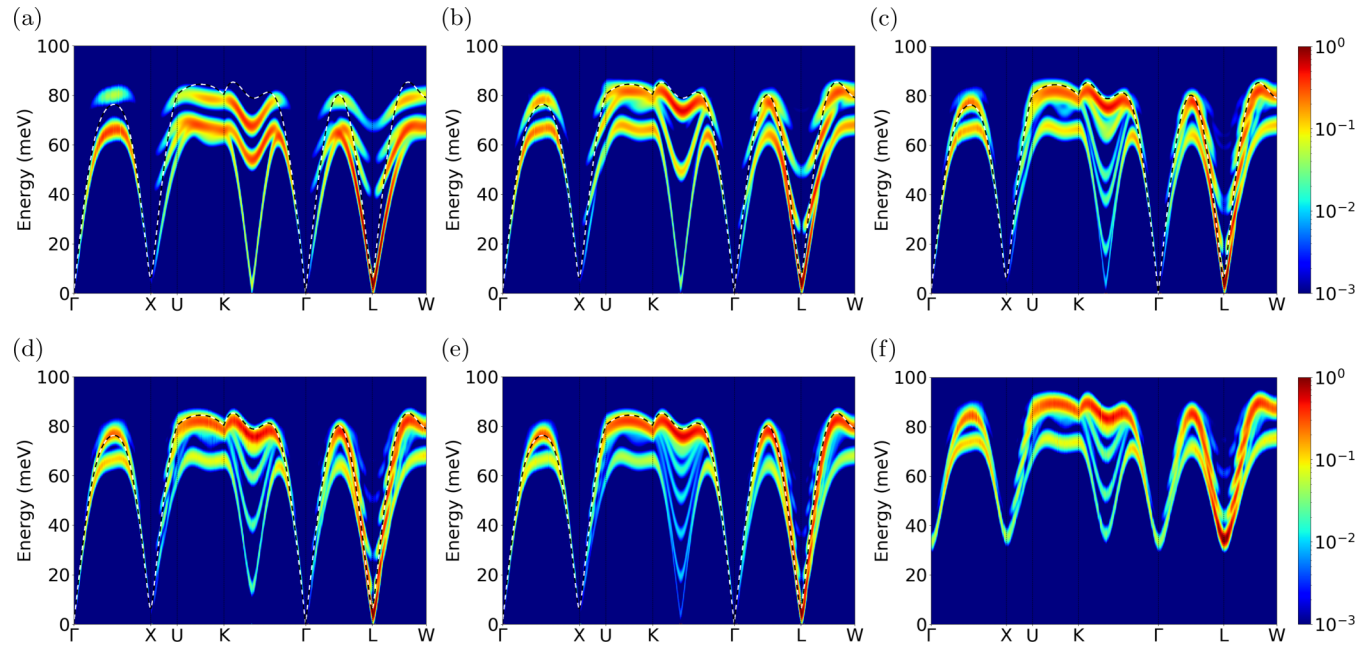

FIG. 4. Spin-scattering function of NiO (100) thin films with (a) 5, (b) 10, (c) 15, (d) 20, and (e) 30 monolayers. (f) 20 Monolayers with an added 5 meV of anisotropy in the direction of the Néel vector which is set to be in the crystallographic direction of confinement, and a temperature of 2K was used for all calculations. A broadening of $\Delta = 1.5$ meV was used.

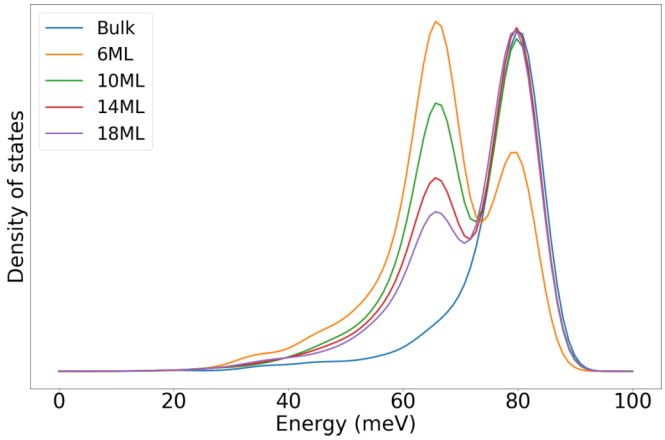

FIG. 5. Density of states of NiO (100) comparing Bulk with varying sizes of thin films. A broadening of $\Delta = 6.5$ meV, was used.

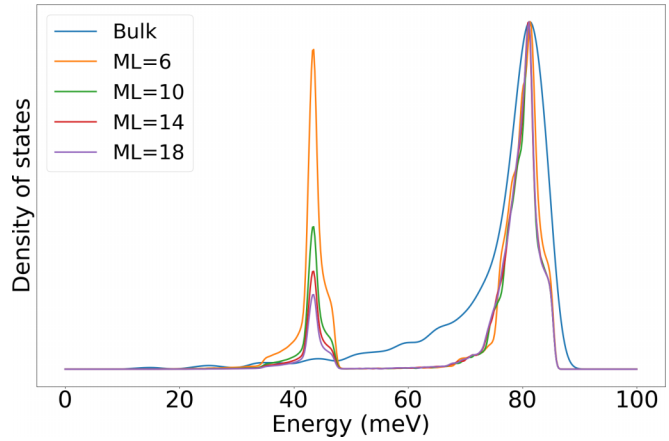

FIG. 7. Density of states of NiO (111) for various film thicknesses. A broadening of $\Delta = 6.5$ meV, was used.

on NiO(111) thin films. Figure 6 shows the spin-scattering function of NiO(111) for 10, 20, 30, 40, and 50 monolayers, alongside the bulk spin-scattering function. We also have included the effect of anisotropy in the case of a 30 ML film with an added anisotropy of 10 meV in the same direction as the Néel vector which is set to be in the crystallographic direction of confinement.

Confinement-induced granularity, due to quasimomentum quantization, appears in different regions of the Brillouin compared to the NiO(100) case, reflecting the crystallographic direction of the confinement. The softer partial interaction mode also appears at lower energies than in NiO(100), with a flatter dispersion. This effect becomes even more apparent when we add an anisotropy in the direction of the Néel vector. A $K = 10$ meV anisotropy leads to the hardening of all modes and a separation between the bulk mode and a confined mode at lower energies, and we observe a flat dispersion across the $\Gamma - L$ path corresponding to the out-of-plane direction, which can therefore be interpreted as a surface-confined mode.

We note also the stark difference between (100) and (111) oriented films in the Γ-X direction. While we see a strong dip in the bulk dispersion for the (100) films, in the (111) films this dip is not present, showing that the direction of confinement can drastically change some of the features of the inelastic response.

Finally, a comparison of the calculated NiO(111) magnon DOS for different film thicknesses is given in Fig. 7. The same tendency as in the NiO(100) films, where the magnon DOS peaks due to the surface-related modes are reduced in intensity and merge into the main bulklike response for (111)

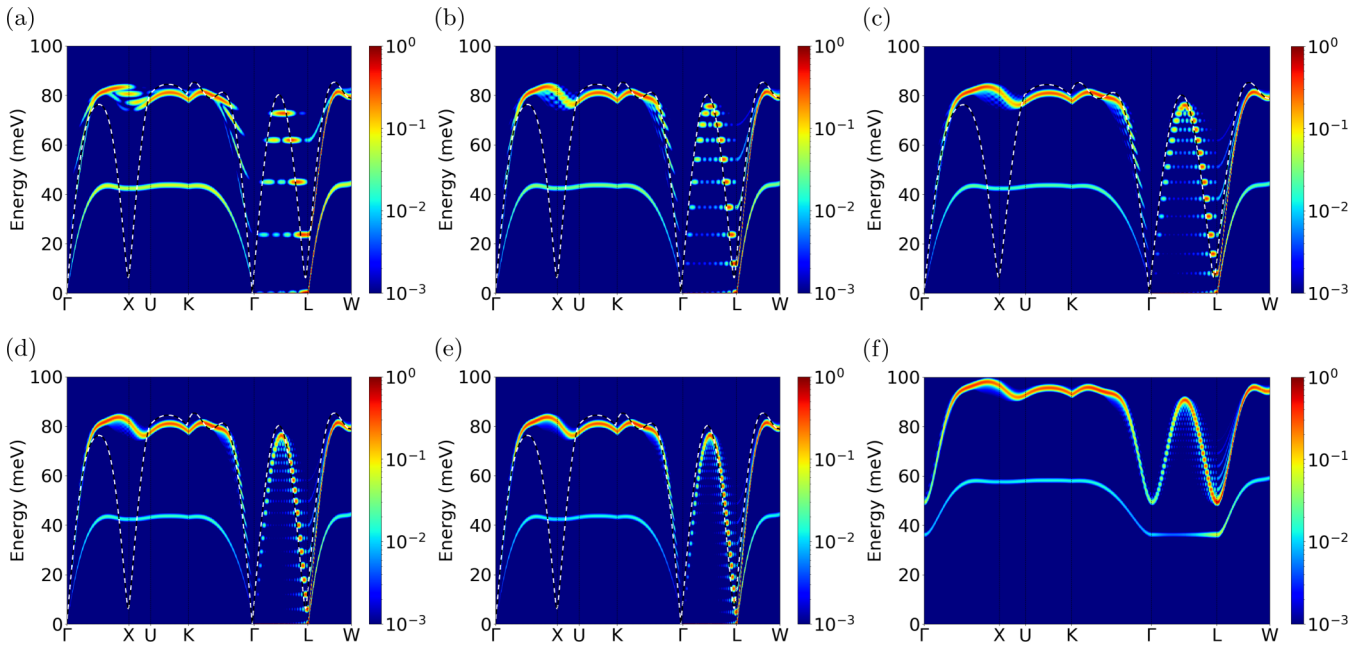

FIG. 6. Spin-scattering function of NiO (111) thin films with (a) 10, (b) 20, (c) 30, (d) 40, and (e) 50 monolayers. (f) 50 monolayers with an added 10 meV of anisotropy in the direction of the Néel vector, and a temperature of 2K was used for all calculations. Broadening used was $\Delta = 0.5$ meV.

films above 10 ML is observed. The main difference with Ni(100) appears in the energy position (42 versus 65 meV) of the surface-related peak which is due to the direction of confinement.

IV. CONCLUSION

We outline a methodology to calculate the spin-scattering function, useful for the calculation of the inelastic scattering by magnons, using a second quantization approach. This allows for a Hamiltonian that includes lower dimensionalities in the systems considered, which is applicable to relevant thin film geometries. The method was used to study thin films of bcc Fe(100) and for NiO the (100) and (111) crystallographic orientations. The calculated results reveal distinct characteristics that emphasize the significance of film thickness and crystal orientation on the magnon modes in these systems. In all cases, the emergence of softer modes related to the partial interaction of the magnetic moments close to the surfaces of the material is observed. The appearance of these softer modes related to confinement is evident in the evaluated magnon density of states, through the emergence of peaks at lower energies, which we ascribe as being related to confinement. Comparing the magnon density of states for two different crystallographic orientations of NiO we observe that the confinement-related peak appears at different energies [65 meV for (100) and 42 meV for (111)], showing the importance of the direction in which dimensionality is reduced. The finite crystal size leads to granularity in the spin-scattering function across various directions in the Brillouin zone, due to the quantization of the quasimomenta. This effect is comparable in the two different crystallographic orientations of NiO, where the granularity appears in the path in reciprocal space that is oriented in the direction of the thin film. Additionally, we demonstrate the role of magnetocrystalline anisotropy in both Fe and NiO films, which leads to an overall hardening of the magnon modes. When anisotropy is only included in surface layers, illustrated in the case of bbc Fe, a shift of the confinement-related magnon DOS peak to higher energies with the increase of the surface anisotropy is seen. Overall, this study contributes to the growing body of knowledge in the field of magnonics and serves as a foundation for future research endeavours aimed at harnessing the unique properties of confined magnon modes for fundamental studies and technological applications.

ACKNOWLEDGMENTS

This project was undertaken on the Viking Cluster, which is a high-performance computing facility provided by the University of York. We are grateful for computational support from the University of York High-Performance Computing service, Viking and the Research Computing team. SuperSTEM is the UK National Research Facility for Advanced Electron Microscopy, supported by the Engineering and Physical Sciences Research Council (EPSRC) through Grant No. EP/W021080/1. We acknowledge financial support from EPSRC via Grant No. EP/V048767/1 and Royal Society Grant No. IES/R1/211016.

[1] A. Mahmoud, F. Ciubotaru, F. Vanderveken, A. V. Chumak, S. Hamdioui, C. Adelmann, and S. Cotofana, Introduction to spin wave computing, J. Appl. Phys. **128**, 161101 (2020).

[2] A. Barman, G. Gubbiotti, S. Ladak, A. O. Adeyeye, M. Krawczyk, J. Gräfe, C. Adelmann, S. Cotofana, A. Naeemi, V. I. Vasyuchka, B. Hillebrands, S. A. Nikitov, H. Yu, D. Grundler, A. V. Sadovnikov, A. A. Grachev, S. E. Sheshukova, J.-Y. Duquesne, M. Marangolo, G. Csaba, W. Porod, V. E. Demidov, S. Urazhdin, S. O. Demokritov, E. Albisetti, D. Petti, R. Bertacco, H. Schultheiss, V. V. Kruglyak, V. D. Poimanov, S. Sahoo, J. Sinha, H. Yang, M. Münzenberg, T. Moriyama, S. Mizukami, P. Landeros, R. A. Gallardo, G. Carlotti, J.-V. Kim, R. L. Stamps, R. E. Camley, B. Rana, Y. Otani, W. Yu, T. Yu, G. E. W. Bauer, C. Back, G. S. Uhrig, O. V. Dobrovolskiy, B. Budinska, H. Qin, S. van Dijken, A. V. Chumak, A. Khitun, D. E. Nikonov, I. A. Young, B. W. Zingsem, and M. Winklhofer, The 2021 magnonics roadmap, J. Phys.: Condens. Matter **33**, 413001 (2021).

[3] B. Lenk, H. Ulrichs, F. Garbs, and M. Münzenberg, The building blocks of magnonics, Phys. Rep. **507**, 107 (2011).

[4] M. Krawczyk and D. Grundler, Review and prospects of magnonic crystals and devices with reprogrammable band structure, J. Phys.: Condens. Matter **26**, 123202 (2014).

[5] L. Sheng, J. Chen, H. Wang, and H. Yu, Magnonics based on thin-film iron garnets, J. Phys. Soc. Jpn. **90**, 081005 (2021).

[6] D. Petti, S. Tacchi, and E. Albisetti, Review on magnonics with engineered spin textures, J. Phys. D **55**, 293003 (2022).

[7] X. S. Wang and X. R. Wang, Topological magnonics, J. Appl. Phys. **129**, 151101 (2021).

[8] C. Etz, L. Bergqvist, A. Bergman, A. Taroni, and O. Eriksson, Atomistic spin dynamics and surface magnons, J. Phys.: Condens. Matter **27**, 243202 (2015).

[9] M. G. Cottam and D. R. Tilley, *Introduction to Surface and Superlattice Excitations* (CRC Press, Boca Raton, FL, 2019).

[10] K. Zakeri, Probing of the interfacial Heisenberg and Dzyaloshinskii–Moriya exchange interaction by magnon spectroscopy, J. Phys.: Condens. Matter **29**, 013001 (2017).

[11] S. Beairsto, M. Cazayous, R. S. Fishman, and R. de Sousa, Confined magnons, Phys. Rev. B **104**, 134415 (2021).

[12] T. Holstein and H. Primakoff, Field dependence of the intrinsic domain magnetization of a ferromagnet, Phys. Rev. **58**, 1098 (1940).

[13] N. N. Bogoljubov, On a new method in the theory of superconductivity, Il Nuovo Cimento **7**, 794 (1958).

[14] E. Simon and L. Szunyogh, Spin-spiral formalism based on the multiple-scattering Green's function technique with applications to ultrathin magnetic films and multilayers, Phys. Rev. B **100**, 134428 (2019).

[15] S. M. Rezende, Theory of coherence in Bose-Einstein condensation phenomena in a microwave-driven interacting magnon gas, Phys. Rev. B **79**, 174411 (2009).

[16] G. Li, C. Sun, T. Nattermann, and V. L. Pokrovsky, Long-wave magnons in a ferromagnetic film, Phys. Rev. B **98**, 014436 (2018).
[17] A. Kreisel, Spin-wave calculations for Heisenberg magnets with reduced symmetry, Ph.D. thesis, Universitätsbibliothek Johann Christian Senckenberg, 2011.
[18] S. V. Halilov, H. Eschrig, A. Y. Perlov, and P. M. Oppeneer, Adiabatic spin dynamics from spin-density-functional theory: Application to Fe, Co, and Ni, Phys. Rev. B **58**, 293 (1998).
[19] J. Kubler, K. H. Hock, J. Sticht, and A. R. Williams, Density functional theory of non-collinear magnetism, J. Phys. F **18**, 469 (1988).
[20] R. S. Fishman, J. A. Fernandez-Baca, and T. Rõõm, *Spin-Wave Theory and its Applications to Neutron Scattering and THz Spectroscopy* (Morgan and Claypool Publishers, San Francisco, CA, 2018), pp. 2053–2571.
[21] F. J. dos Santos, M. dos Santos Dias, F. S. Mendes Guimarães, J. Bouaziz, and S. Lounis, Spin-resolved inelastic electron scattering by spin waves in noncollinear magnets, Phys. Rev. B **97**, 024431 (2018).
[22] S. M. Rezende, *Quantum Theory of Spin Waves: Magnons* (Springer International Publishing, Cham, 2020), pp. 71–134.
[23] W. Nolting and A. Ramakanth, *Quantum Theory of Magnetism* (Springer, Berlin, 2009).
[24] C. Lee, D. Vanderbilt, K. Laasonen, R. Car, and M. Parrinello, *Ab initio* studies on the structural and dynamical properties of ice, Phys. Rev. B **47**, 4863 (1993).
[25] S. V. Meshkov, Low-frequency dynamics of Lennard-Jones glasses, Phys. Rev. B **55**, 12113 (1997).
[26] M. Pajda, J. Kudrnovský, I. Turek, V. Drchal, and P. Bruno, *Ab initio* calculations of exchange interactions, spin-wave stiffness constants, and Curie temperatures of Fe, Co, and Ni, Phys. Rev. B **64**, 174402 (2001).
[27] F. L. Durhuus, T. Skovhus, and T. Olsen, Plane wave implementation of the magnetic force theorem for magnetic exchange constants: Application to bulk Fe, Co, and Ni, J. Phys.: Condens. Matter **35**, 105802 (2023).
[28] C. Kittel, *Introduction to Solid State Physics*, 8th ed. (Wiley, New York, NY, 2004).
[29] M. Hafez-Torbati, F. B. Anders, and G. S. Uhrig, Simplified approach to the magnetic blue shift of Mott gaps, Phys. Rev. B **106**, 205117 (2022).
[30] M. T. Hutchings and E. J. Samuelsen, Measurement of spin-wave dispersion in NiO by inelastic neutron scattering and its relation to magnetic properties, Phys. Rev. B **6**, 3447 (1972).
[31] N. Rinaldi-Montes, P. Gorria, D. Martínez-Blanco, A. B. Fuertes, L. Fernández Barquín, J. R. Fernández, I. de Pedro, M. L. Fdez-Gubieda, J. Alonso, L. Olivi, G. Aquilanti, I. Puente-Orench, and J. A. Blanco, On the exchange bias effect in NiO nanoparticles with a core(antiferromagnetic)/shell (spin glass) morphology, J. Phys.: Conf. Ser. **663**, 012001 (2015).